Applied Catalysis B: Environmental 322 (2023) 122086

Contents lists available at ScienceDirect

Applied Catalysis B: Environmental

journal homepage: www.elsevier.com/locate/apcatb

Natural leaf-inspired solar water splitting system

Wonjoo Jin [a,b,1], Changhwan Shin [a,1], Seyeon Lim [a], Kangmin Lee [a], Je Min Yu [a,c], Kwanyong Seo [a,d,*], Ji-Wook Jang [a,c,d,*]

[a] School of Energy and Chemical Engineering, Ulsan National Institute of Science and Technology (UNIST), Ulsan 44919, Republic of Korea
[b] Max Planck Center for Attosecond Science, Max Planck POSTECH/KOREA Research Initiative, Pohang, Gyeongbuk 37673, Republic of Korea
[c] Emergent Hydrogen Technology R&D Center, Ulsan National Institute of Science and Technology (UNIST), Ulsan 44919, Republic of Korea
[d] Graduate School of Carbon Neutrality, Ulsan National Institute of Science and Technology (UNIST), Ulsan 44919, Republic of Korea

ARTICLE INFO

Keywords:
Water splitting
Crystalline silicon
Artificial leaf
Photoelectrochemical cell
Interdigitated back contact (IBC)

ABSTRACT

We designed a monolithic artificial leaf that mimics a natural leaf; the artificial leaf has a crystalline silicon (c-Si) interdigitated back contact (collectively, c-Si IBC) structure. On the front-side of the artificial leaf, the c-Si module acts similar to chlorophyll in natural leaves, converting solar energy into photo-carriers. On the rear-side of the artificial leaf, a hydrogen and oxygen evolution catalyst converts the carriers into hydrogen; this occurs without blocking light, similar to the conversion of photo-carriers into chemical energy, which mostly occurs on the backside of natural leaves. The solar-to-hydrogen conversion efficiency of the c-Si IBC photoanode and artificial leaf was 10.1% and 8.4% respectively, which are higher than that of a natural leaf (0.1–1%).

1. Introduction

Photoelectrochemical (PEC) water splitting technology is one of the most promising eco-friendly methods to generate hydrogen [1]. This technology resembles natural photosynthesis; in natural photosynthesis, solar energy is transformed into chemical energy (via sugar or starch), whereas in PEC water splitting technology, solar energy is transformed into hydrogen [2,3]. Because of this similarity, there have been several studies of mimicking natural photosynthesis to increase the solar-to-hydrogen conversion (STH) efficiency of the PEC water splitting system [4–6]. Recently, there have been many efforts to develop the wireless PEC system known as the "artificial leaf" [7–9] owing to its potential for showing high STH efficiency compared to the wired PEC system and PV-EC system (photovoltaic (PV) combined with electrolysis (EC) system) particularly in the scaled-up photoelectrode due to the minimized ohmic loss (from wireless configuration). Furthermore, the simplified monolithic design of the artificial leaf system can also reduce the installation cost, and requires less space compared to the wired PEC system as well as PV-EC system [9–13].

In most studies, Si has been applied as a promising PEC water splitting material, owing to its high abundance on earth and efficiency in utilizing solar energy due to its appropriate bandgap (1.1–1.7 eV; varies depending on crystallinity) [14–17]. However, there are two critical problems in using Si for hydrogen generation; first, the output voltage of the Si photovoltaic device (0.6–0.9 V) is still much lower than the potential required for water splitting (1.5–1.8 V). Second, Si is not stable in a basic electrolyte condition; thus, an Si-based device is not efficient in leading a water splitting reaction in water. For these reasons, applying oxygen evolution reaction (OER) and hydrogen evolution reaction (HER) catalysts on Si electrodes and the multi-junction of Si unit cells have been essential for achieving efficient water splitting [18].

Nocera et al. [9] were the first to demonstrate the "artificial leaf," which is the stand-alone PEC water splitting device, with Si. They employed a triple-junction amorphous silicon (a-Si) solar cell and

Abbreviations: a-Si, amorphous silicon; BSF, back surface field; c-Si IBC, crystalline silicon interdigitated back contact; *FF*, fill factor; GC, gas chromatography; HER, hydrogen evolution reaction; J_{SC}, short-circuit current density; *J-E*, current density-potential; KPi, potassium phosphate; LSV, linear sweep voltammetry; NOA 63, Norland optical adhesive 63; OER, oxygen evolution reaction; PCE, power conversion efficiency; PE-CVD, plasma enhanced chemical vapor deposition; PEC, photoelectrochemical; PV, photovoltaic; RHE, reversible hydrogen electrode; SEM, scanning electron microscopy; STH, solar-to-hydrogen conversion; XPS, X-ray photoelectron spectroscopy; V_{OC}, open-circuit voltage.

* Corresponding authors at: School of Energy and Chemical Engineering, Ulsan National Institute of Science and Technology (UNIST), Ulsan 44919, Republic of Korea

E-mail addresses: kseo@unist.ac.kr (K. Seo), jjwjang@unist.ac.kr (J.-W. Jang).

[1] These authors contributed equally to this work.

https://doi.org/10.1016/j.apcatb.2022.122086
Received 16 July 2022; Received in revised form 21 September 2022; Accepted 17 October 2022
Available online 20 October 2022

deposited a cobalt borate OER catalyst and NiMoZn HER catalyst on the front-side and rear-side of the artificial leaf, respectively. The STH efficiency of that artificial leaf was 2.5% [9]. Xiang and Lewis et al. [7] utilized the same triple-junction a-Si structure with Co-Pi OER and Pt HER catalysts deposition on the front-side and rear-side of the artificial leaf, respectively, and recorded a 3.2% STH efficiency [7]. Bogdanoff et al. [8] also utilized a triple-junction Si solar cell structure consisting of two a-Si and one microcrystalline Si components to fabricate an artificial leaf. A Pt HER catalyst was directly loaded on the rear-side of the artificial leaf, but an opaque RuO_2 OER catalyst on Ti foil was positioned outside of the Si solar cells. The STH efficiency of that artificial leaf was 3.4% [8].

In the abovementioned studies, the most critical problem is that OER or HER catalysts on Si block the incident light, which reduces the overall efficiency of the artificial leaf [7,9,14]. Although they are not directly coated on the Si surface, but rather are positioned outside of the Si solar cell, an additional amount of area is thus required, such that the efficiency is reduced [8]. In a natural leaf, however, most of the chlorophyll is positioned on its front-side, which transforms solar energy into photo-carriers; notably, the chemical reactions which convert the photo-carriers into the chemical energy of carbohydrates mainly occur on the rear-side of the natural leaf, and thus do not block the incident light. Moreover, these chemical reactions do not occur outside of the area of the natural leaf itself [19–21].

In this study, we propose an artificial leaf to mimic the structure of the natural leaf; the artificial leave has a crystalline silicon (c-Si) interdigitated back contact (collectively, c-Si IBC) structure consisting of a front-side positioned c-Si, which transforms solar energy into photo-

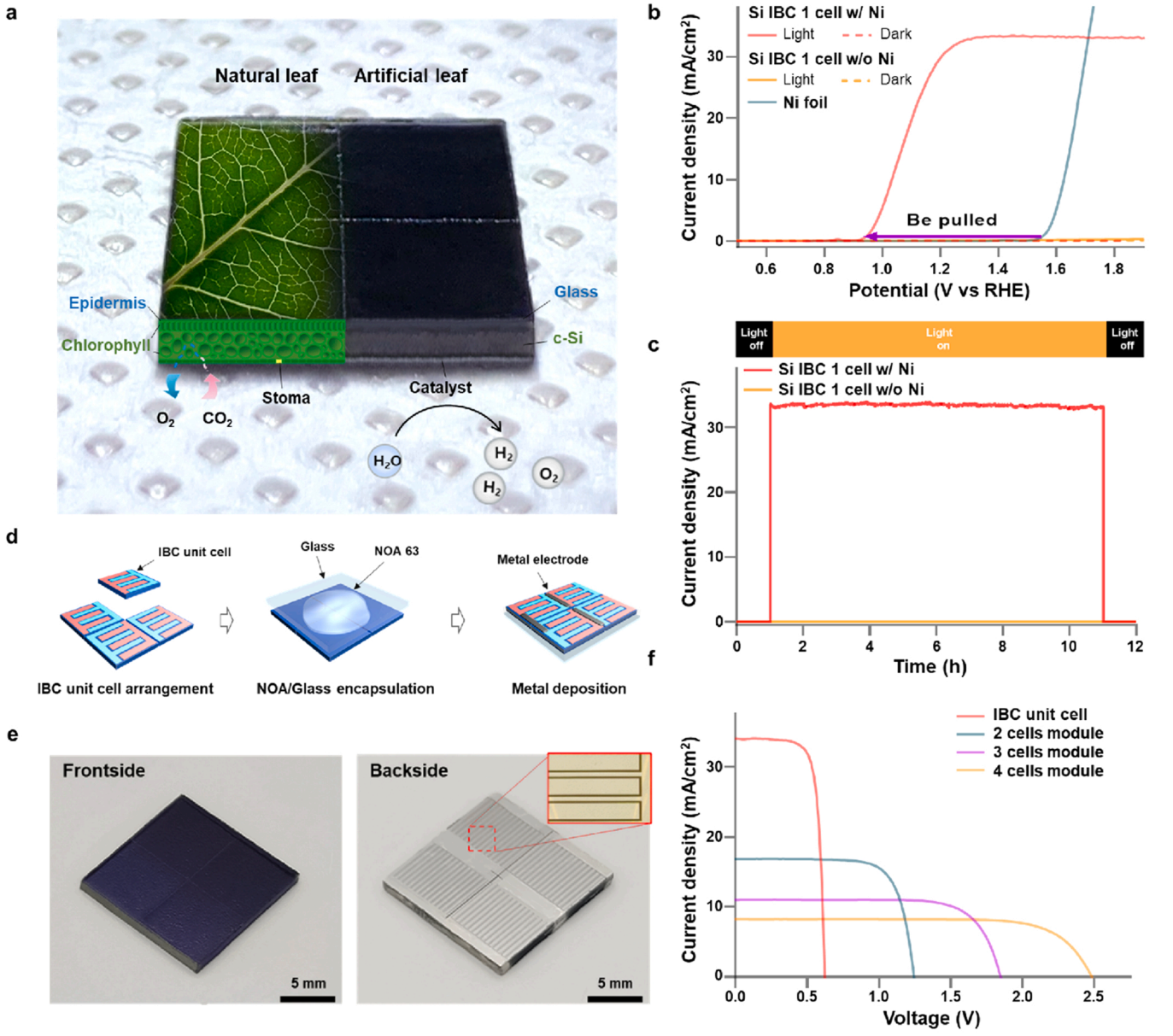

Fig. 1. Structure of the artificial leaf designed in our study and its properties. a, Schematic comparison of natural leaf and the c-Si interdigitated back contact (c-Si IBC) artificial leaf. b, Comparison of current density-potential (*J-E*) curves of c-Si IBC unit cell photoanode with Ni foil (Si IBC 1 cell w/ Ni; red), without Ni foil (Si IBC 1 cell w/o Ni; orange) under AM 1.5 G illumination (100 mW/cm^2), and Ni foil anode (cyan) in dark conditions in 1 M NaOH electrolyte (pH 13.8). c, Chronoamperometry tests of c-Si IBC unit cell photoanode at 1.5 V vs. RHE. d, Fabrication process of c-Si IBC module. e, Photographs of c-Si IBC module front side and rear-side. f, Photovoltaic performance of c-Si IBC unit cell (red), 2 cells (cyan), 3 cells (purple), and 4 cells (orange) module under AM 1.5 G solar illumination. The series-connected modules consisting of 2, 3, and 4 c-Si IBC unit cells are denoted by the 2, 3, and 4 cells module, respectively; reversible hydrogen electrode (RHE), Norland optical adhesive 63 (NOA 63).

carriers similar to chlorophyll, and rear-side positioned OER and HER catalysts that convert the photo-carriers into hydrogen (Fig. 1a). Because the OER and HER catalysts are positioned at the bottom, they do not block the light, thus, the optical properties of the catalyst need not be considered, which has been a critical limitation in previous studies that applied OER and HER catalysts on photoelectrodes. By mimicking the natural leaf, the proposed structure offers an efficient and scalable system architecture to address the long-standing challenges of PEC water splitting technology.

2. Experimental

2.1. Fabrication of crystalline silicon interdigitated back contact (c-Si IBC) solar cell

The c-Si IBC solar cell was fabricated using a P-type Si wafer having a resistivity of 1–3 Ω·cm and thickness of 120 μm. The c-Si IBC solar cells were designed using both an emitter (n^+) and a back surface field (BSF; p^+) at the rear surface of the solar cells. To develop the emitter and the BSF region, respectively, an SiO_2 barrier was required. Therefore, 900-nm thick SiO_2 films were deposited on both the front-side and rear-side of the Si substrate through plasma enhanced chemical vapor deposition (PE-CVD; PEH-600, SORONA, Korea). To form the patterned diffusion barrier for the emitter contact, the SiO_2 film on the backside of the substrate was patterned using the photolithography and SiO_2 etch-back process. The heavily-doped region (n^+) was formed by phosphorus diffusion via the spin-on-dopant (P509, Filmtronics, USA). The doping process of the boron dopant was conducted in a tube furnace, with mixed ambient air of 20% O_2 and 80% N_2 at 900 °C. The sheet resistance of the n^+-Si region was 100–150 Ω /sq. The SiO_2 diffusion barrier and phosphate, the excess of which remained behind after the spin-on-doping diffusion, were removed using diluted HF solution. The entire surface, except for the emitter and BSF regions, was coated with a 10-nm thick Al_2O_3 layer at 200 °C, through the atomic layer deposition method (Atomic premium, CN1), and a 60 nm-thick SiN_x film was deposited at 350 °C using PE-CVD (PEH-600, SORONA, Korea). Then, a BSF region was selectively patterned through photolithography, and 10 nm MoO_x/500 nm Al was deposited via a thermal evaporation process. For the emitter metal electrode, an interdigitated grid pattern in the emitter region was developed by photolithography, and a 500-nm thick Al film was thermally deposited.

2.2. Fabrication of c-Si IBC solar module

For the modularization process, we used the manufactured c-Si IBC unit cell. We arranged 2–4 unit cells for series connection to the glass substrate. The c-Si IBC unit cell and glass were contacted using a transparent ultraviolet-curable polymer (NOA 63, Norland Products, Inc. Spain). Then, an Al contact electrode was fabricated between the unit cells through a thermal evaporation process. Through that process, the emitter of one c-Si IBC unit cell and the BSF part of another c-Si IBC unit cell were modularized by serial connection.

2.3. Characterization of c-Si IBC solar cell and c-Si solar module

The photovoltaic properties of our solar cells were investigated using a solar simulator (Class AAA, Oriel Sol3A, Newport, USA) under the illumination of AM 1.5 G. The incident flux was measured using a calibrated power meter and double-checked using a National Renewable Energy Laboratory calibrated solar cell (PV Measurements, Inc. USA). The external quantum efficiency was measured using a Xe light source and a monochromator in the wavelengths of 400–1100 nm. Optical reflection measurements were performed over the wavelengths of 400–1100 nm, using a ultraviolet-visible near infrared spectrophotometer (Cary 5000, Agilent, USA) equipped with a 110 mm integrating sphere to account for the total light (diffused and specular) reflected from the samples.

2.4. Fabrication and characterization of photoelectrodes

To fabricate c-Si IBC photoelectrodes, the interdigitated n- and p-type doped regions on the rear-side of the c-Si unit cell or modules were passivated by NOA 63, and Ni foil (0.1 mm thick, 99.5%, Alfa Aesar, USA) was attached to the remaining p-type region on the rear-side of the c-Si using Ag paste (Elcoat P-100, CANS, Japan). Then, either a Cu wire was attached to the remaining n-type region of the c-Si using the Ag paste to make a photoanode, or the Ni foil was attached to the remaining n-type region to make an artificial leaf. Next, the areas of the c-Si photoelectrodes (except for the front-side light-receiving area and rear side water-splitting reaction area) were covered by NOA 63 and epoxy (JB Weld, USA). To use Pt for HER in the c-Si artificial leaf devices, Pt was sputtered on the Ni foil side, which was then attached to the n-type region on the rear-side of the artificial leaf, using a sputter (EMITECH K575X, Tescan, Czech Republic) for 30 s at 20 mA. X-ray photoelectron spectroscopy (XPS, K-alpha, ThermoFisher, USA) measurements were carried out to analyze the chemical compositions of the Ni surface on the c-Si IBC photoanodes. All XPS sample data were calibrated using the adventitious C-C binding energy of 284.8 eV in the XPS C 1 s spectrum. The images of scanning electron microscopy (SEM) were observed using an S-4800 cold field-emission scanning electron microscopy (Hitachi High-Technologies, Japan). An inductively coupled plasma optical emission spectrometer (iCAP-Pro, ThermoFisher, USA) was used to quantify the Ni content in electrolytes before and after PEC experiments of the c-Si IBC photoanodes.

2.5. Photoelectrochemical (PEC) and electrochemical measurement

All PEC and electrochemical measurements were conducted in 1 M NaOH (98%, pellets, Alfa Aesar, USA) electrolyte (pH 13.8) unless otherwise noted, with continuous Ar gas (99.999%) purging. The PEC measurements of the c-Si IBC photoanodes and artificial leaf devices were carried out at the illumination of AM 1.5 G (1 sun) from a solar simulator (10500, Abet Technologies, USA); the light intensity was calibrated with an Si reference cell (PEC-SI01, Peccell Technologies, Inc., Japan). A Pt rod was used as the counter electrode for the 2- and 3-electrode systems and an Hg/HgO reference electrode (RE-61AP, ALS, Japan) was used for the 3-electrode system, with an Ivium-n-Stat Multichannel potentiostat. Linear sweep voltammetry (LSV) measurements were carried out at a scan rate of 20 mV/s. to represent current density-potential curves.

2.6. Analysis of gas products

The gas products were measured in a one-compartment stainless-steel sealed reactor having one gas inlet and one gas outlet. During the measurements, Ar gas flowed to the reactor (as the carrier gas) at the rate of 10 standard cm^3 per minute, through a mass flow controller (5850E, Brooks, USA). The gas outlet of the reactor was connected to a gas chromatography (GC) equipment (6500GC system, YL Instrument, Korea) by a polytetrafluoroethylene line; therefore, the gas products from the reactor flowed to the GC equipment with the Ar carrier gas, after passing through a water filter (202234-B, Chromatography Research Supplies, Inc., USA), which was installed at the front of the GC equipment.

3. Results and discussion

3.1. Design and fabrication of c-Si IBC photoanode

To enable the seamless structural connection of the c-Si solar cell and the HER and OER catalysts, the c-Si IBC solar cells were designed with an all back-contact structure, where both the emitter and BSF were

positioned at the rear surface, unlike conventional solar cells, which have the emitter and BSF positioned at the front and rear surfaces, respectively [22]. The detailed fabrication process of the c-Si IBC solar cell was described above in the Experimental section and is presented in Fig. S1 (Supplementary Material). The best device exhibits a short-circuit current density (J_{SC}) of 34.3 mA/cm^2 under an illumination of AM 1.5 G (100 mW/cm^2), which matches with the sum of the external quantum efficiency of the c-Si IBC unit cell (Fig. S2, Supplementary Material). To fabricate the c-Si IBC-based photoanode, we attached Ni foil on the rear-side of c-Si IBC. We used Ni foil (~100 μm thickness) not only to protect the c-Si IBC from the basic electrolyte but also to use it as a catalyst. The Ni foil helps in allowing the efficient transport of the photo-carriers from the c-Si IBC solar cell to the water, because the Ni surface is transformed to Ni oxyhydroxide (NiOOH), which is known to be an active OER catalyst in a basic electrolyte [23,24]. The front-side of the c-Si IBC photoanode was protected using a glass substrate to improve the stability of the device in the basic electrolyte environment, similar to the way in which the epidermis protects the chloroplast in the natural leaf structure (Fig. 1a). As shown in Fig. 1b, the c-Si IBC unit cell photoanode portrayed an onset potential of 0.95 V at 1 mA/cm^2, which was more positively shifted than that of the Ni foil (by 0.61 V). This was well-matched with the open-circuit voltage (V_{OC}) of the c-Si IBC unit cell (0.62 V). The saturated photocurrent density of the c-Si IBC unit cell photoanode (~33.3 mA/cm^2) was slightly lower than the J_{SC} value (34.3 mA/cm^2) of the c-Si IBC unit cell, indicating a small optical loss, due to the glass reflection on the top of the c-Si IBC unit cell photoanode. The fabricated c-Si IBC photoanode showed stable performance for 10 h at 1.5 V vs. the reversible hydrogen electrode (RHE) in 1 M NaOH under an illumination of AM 1.5 G, without observable photocurrent loss during the measurement (Fig. 1c). However, the photocurrent density of the photoanode without the Ni foil was only 64 μA/cm^2 at 1.23 V vs. RHE, and it lost its activity within a few minutes, indicating the essential role of Ni foil in protecting the c-Si from the basic electrolyte and facilitating the efficient charge transfer for the OER reaction (Fig. 1b, c and Fig. S3, Supplementary Material).

In order to determine the PEC performances and stabilities of the c-Si IBC unit cell photoanode under different pH conditions, we performed current density-potential (*J-E*) measurements and chronoamperometry tests (at 1.5 V vs. RHE) (Fig. S4, Supplementary Material). We selected 1 M NaOH (pH 13.8), 0.5 M potassium phosphate (KPi) buffer (pH 7.00), and 0.5 M H_2SO_4 (pH 0.78) electrolytes as representative electrolytes with high pH, neutral pH, and low pH, respectively. The c-Si IBC photoanode showed a performance decrease in low pH conditions because the Ni which was used as the OER catalyst material in the c-Si IBC photoanode was unstable in the acidic electrolytes [25]. In the neutral electrolyte, the photoanode showed a low but relatively stable performance (i.e., positive onset potential and poor fill factor [*FF*]). In the basic electrolyte, it showed a stable performance during the chronoamperometry test for 10 h with good onset potential and *FF* (Fig. S4, Supplementary Material). To observe the change in the morphology of the Ni foil after the stability tests under three different pH conditions, we conducted SEM analysis (Fig. S5, Supplementary Material). In the basic electrolyte, the morphology of the Ni foil after the stability test was almost unchanged compared to that before the stability test. However, the Ni foil surface in the neutral and acidic electrolytes changed noticeably after the stability test, becoming rough and etched, indicating the leaching of Ni. To further verify the stability, we performed inductively coupled plasma optical emission spectroscopy (ICP-OES) measurements in the electrolyte after the stability test (Table S1). In the basic electrolyte, no Ni metal was detected (i.e., the concentration of Ni was below the detection limit of the equipment: 0.0010 mg/L), while a significant amount of Ni was detected in the acidic electrolyte (398.403 mg/L) and to some extent in the neutral electrolyte (45.865 mg/L).

Furthermore, XPS was conducted to investigate the chemical status of Ni surface on the Ni foil of c-Si IBC photoanode before and after PEC experiments in the basic electrolyte (Fig. S6, Supplementary Material). The high-resolution Ni 2p spectrum of the c-Si IBC photoanode before PEC experiments shows Ni $2p_{3/2}$ and Ni $2p_{1/2}$ peaks by spin-orbit splitting, in which the deconvoluted Ni $2p_{3/2}$ peaks appear at 852.3 eV, 853.4 eV, and 858.1 eV, corresponding to Ni^0 in metallic Ni, Ni^{2+} in NiO, and a satellite peak, respectively [26–28]. After the PEC LSV measurements, the Ni $2p_{3/2}$ peaks became dominant at 855.3 eV and 856.2 eV, which indicates Ni^{2+} in $Ni(OH)_2$ and Ni^{3+} in NiOOH, respectively [27–31]. The samples after the PEC stability tests of 1 h and 10 h show consistent Ni 2p spectrums with the main Ni $2p_{3/2}$ peaks at 855.3–4 eV and 856.1–3 eV. This result indicates that the Ni surface of c-Si IBC photoanode was transformed to $Ni(OH)_2$ and NiOOH, and was well maintained during the PEC OER measurements.

The V_{OC} of the c-Si IBC unit cell photoanode (0.62 V) was not enough for unassisted water splitting; at least 1.5–1.8 V of photovoltage is required, considering the thermodynamic potential of water splitting (1.23 V) and its overpotential [5,6]. Therefore, we fabricated a solar module of c-Si IBC unit cells. The method of modularization was described in the Experimental section above and is presented in Fig. 1d. One c-Si IBC unit cell emitter area and the BSF area of the other c-Si IBC unit cell were connected in series. In this way, the c-Si solar module was fabricated by interconnecting 2–4 units of c-Si mini-cells in series, and it demonstrated a high output voltage of ~2.4 V (Fig. 1f). As shown in Fig. 1e, the optical image of the module manufactured in this way clearly shows that it does not require unnecessary space for connecting the unit cells; thus, the module can be manufactured with a seamless structure. Fig. 1f portrays the current density-voltage curve of the c-Si IBC module under AM 1.5 G illumination. All photovoltaic parameters, such as J_{SC}, V_{OC}, *FF*, and power conversion efficiency (PCE) are summarized in Table 1. The c-Si IBC module (consisting of 2–4 cells) portrayed a V_{OC} of 1.2 V, 1.8 V, and 2.4 V. Because the series-connected modules consisting of 3 or 4 c-Si IBC unit cells possessed enough photovoltages for the overall PEC water splitting reaction, we selected those cells to fabricate the photoanode.

To demonstrate the c-Si IBC module photoanode, the p-type doped and n-type doped regions on the rear-side of the c-Si IBC module were individually, directly connected to the Ni foil and Cu wire using Ag paste, respectively, forming a wired PEC system having a Pt rod cathode for HER (Fig. 2a). To evaluate the unassisted solar water splitting performances of the c-Si IBC module photoanodes, the PEC measurements were carried out in a 2-electrode configuration, without a reference electrode. The PEC performances of the 3-electrode system are shown in Fig. S7 (Supplementary Materials). We performed the LSV measurements for the c-Si IBC 3 cells and 4 cells module photoanodes in 1 M NaOH electrolyte under an illumination of AM 1.5 G. The negative onset potentials of − 0.21 V and − 0.74 V at 1 mA/cm^2 for the 3 cells and 4 cells module photoanodes, respectively, clearly indicated that the PEC water splitting reaction could occur without external bias (Fig. 2b). The saturated currents of the photoanodes were about 10.4 mA/cm^2 for the c-Si IBC 3 cells module photoanode and about 8.35 mA/cm^2 for the c-Si

Table 1
Summary of electrical performance of c-Si IBC modules (unit cell, 2 cells, 3 cells, and 4 cells module). The tables in brackets indicate the mean performance of the four devices.

Device	J_{SC} (mA/cm^2)	V_{OC} (V)	*FF* (%)	PCE (%)
c-Si IBC unit cell	34.3 (34.1)	0.62 (0.61)	76.9 (76.5)	16.3 (15.9)
c-Si IBC 2 cells module	16.4 (16.2)	1.24 (1.23)	76.7 (75.7)	15.7 (15.1)
c-Si IBC 3 cells module	11.1 (11.0)	1.84 (1.82)	77.6 (76.1)	15.8 (15.2)
c-Si IBC 4 cells module	8.4 (8.3)	2.46 (2.44)	75.1 (74.6)	15.5 (15.1)

*Note: crystalline silicon interdigitated back contact (c-Si IBC).

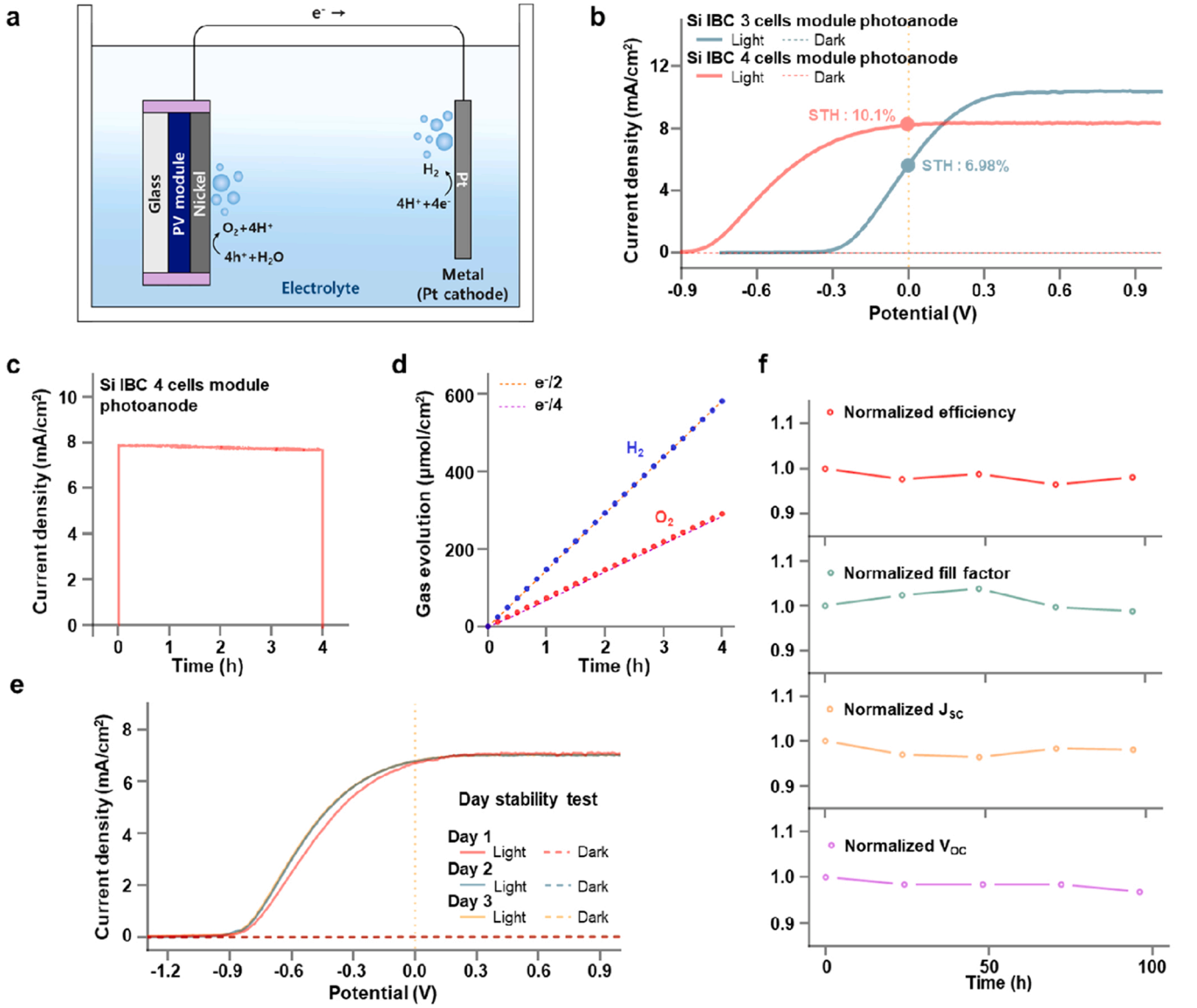

Fig. 2. Photoelectrochemical (PEC) water splitting performances using crystalline silicon interdigitated back contact (c-Si IBC) module photoanode. a, Schematic illustration of wired PEC system using c-Si IBC module photoanode and Pt cathode for unassisted solar water splitting. b, *J-E* curves of c-Si IBC 3 cells module photoanode (cyan) and 4 cells module photoanode (red) in the 2-electrode configuration with a Pt rod counter electrode in 1 M NaOH electrolyte under 1 sun illumination. c, Chronoamperometry test of c-Si IBC 4 cells module photoanode at 0 V in 1 M NaOH electrolyte under 1 sun illumination, except for 1 min of the initial and end of the test in dark conditions. d, The accumulated amounts of charges (e^-) and hydrogen (H_2) and oxygen (O_2) gases generated during the chronoamperometry test at 0 V in 1 M NaOH under 1 sun illumination; $e^-/2$ (yellow dotted line), $e^-/4$ (violet dotted line), H_2 (blue circle), O_2 (red circle). e, *J-E* curves for the long-term periods of the c-Si IBC 4 cells module photoanode. f, Photovoltaic performances measurement in the long-term periods; photovoltaic (PV), silicon interdigitated back contact (c-Si IBC).

IBC 4 cells module photoanode, almost one-third and one-quarter of the saturated current of the single cell photoanode (33.3 mA/cm^2), respectively, (Figs. 1f and 2b). These results indicated that there was no significant ohmic or optical loss after the fabrication of module based photoelectrodes. Using the operating photocurrents of the c-Si IBC module photoelectrodes, we calculated the STH efficiency (η_{STH}) from the following equation:

$$\eta_{STH} = \frac{J_{OP} \times (1.23 \quad V) \times \eta_{FE}}{P_{in}} \times 100\% \tag{1}$$

where J_{OP} is the operating photocurrent density of a photoelectrode in a 2-electrode configuration without external bias, η_{FE} is the Faradaic efficiency of the hydrogen evolution reaction, and P_{in} is the light intensity illuminated on the photoelectrode (100 mW/cm^2; AM 1.5 G illumination). As shown in Fig. 2b, the photocurrent densities of the c-Si IBC 3 cells and 4 cells module photoanodes at 0 V were 5.67 mA/cm^2 and 8.21 mA/cm^2, which corresponded to the STH efficiencies of 6.98% and 10.1%, respectively. Notably, the c-Si IBC photoanode was stable for 4 h, without a significant loss in its performance, with the Faradaic efficiency being close to 100% for both the HER and OER reactions (Fig. 2c and d). Moreover, there was no noticeable change in the *J-E* curves of the c-Si IBC 4 cells module photoanode for a period 3 days (Fig. 2e). Also, the photovoltaic parameters of the c-Si IBC module in the photoanode, including PCE, *FF*, J_{SC} and V_{OC}, were all consistent, without any noticeable decrease during several days under 1 sun illumination (Fig. 2f).

3.2. Fabrication of artificial leaf

Finally, we fabricated the c-Si IBC module-based wireless all-in-one PEC device, the proposed "artificial leaf" of this study. The detailed scheme of the artificial leaf system is described in Fig. 3a and b. The c-Si IBC 4 cells module was used to fabricate the artificial leaf device, based on the higher performances of the c-Si IBC 4 cells module photoanode (compared to the 3 cells module photoanode) at 0 V (Fig. 2b). The Ni foil was attached to the p-type doped region on the rear-side of the c-Si IBC module, and the HER catalyst was directly attached to the n-type doped region of the c-Si IBC module, without a Cu wire connection. Thus, we developed a wireless PEC system. The real image and operation of the unassisted solar water splitting reaction from the artificial leaf under light illumination are shown in Fig. 3c and Videos 1 and 2 (Supplementary Material).

Because the Ni foil is transformed to $Ni(OH)_2$ and NiOOH in the basic solution as described previously, without additional catalyst loading on the Ni foil, the $Ni(OH)_2$ and NiOOH composite acts collectively as the OER and HER catalysts. In this case, the STH efficiency was about 5.9% (Fig. S8, Supplementary Materials). To further increase the STH efficiency, we used Pt-sputtered Ni foil, instead of bare Ni foil, because Pt has a better catalytic HER performance compared with Ni, as shown in Fig. S9 (Supplementary Materials). When Ni foil and Pt sputtered Ni foil were used as the OER and HER catalysts, respectively, the STH efficiency increased to 8.4% (Fig. 3d). The amount of hydrogen and oxygen evolution indicated a linear increase with their ratio of two, indicating the stable performance of the c-Si IBC-based artificial leaf (Fig. 3e). Notably, the observed STH efficiency of the artificial leaf (8.4%) is higher than that of a natural leaf (0.1–1%), and even higher than those of C4 plants (4.3–6%), which have the record of highest efficiency in terms of photosynthesis among all plants [32,33].

4. Conclusion

In this study, we demonstrated the high performance of a c-Si IBC artificial leaf that was inspired from a natural leaf. Notably, the c-Si module and water splitting catalyst were positioned on the front-side and rear-side of the leaf, respectively, minimizing the efficiency loss

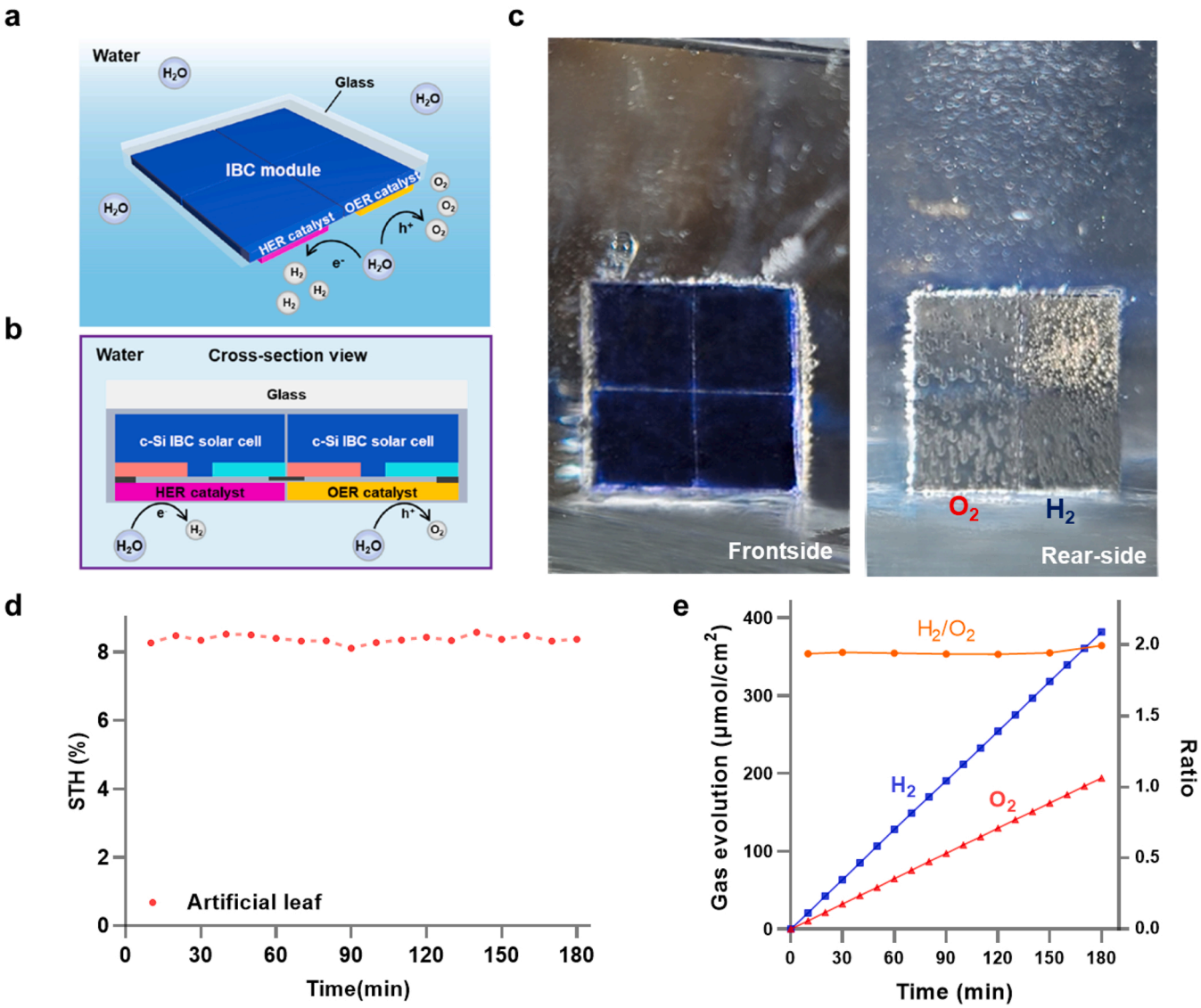

Fig. 3. Unassisted solar water splitting performances using the c-Si IBC artificial leaf device. a, Schematic illustration of unassisted solar water splitting using the artificial leaf device. b, Schematic illustration of the side view of the artificial leaf device. c, Photographs of the unassisted solar water splitting reaction of the artificial leaf under light illumination in 1 M NaOH electrolyte. d, Solar-to-hydrogen (STH) efficiency converted from hydrogen gas evolved from the artificial leaf under 1 sun illumination in the 1 M NaOH electrolyte. e, The accumulated amounts of hydrogen (blue) and oxygen (red) gases evolved from the artificial leaf and the gas ratio (orange); crystalline Si (c-Si), interdigitated back contact (IBC), hydrogen evolution reaction (HER), oxygen evolution reaction (OER).

due to light absorption by or reflection from the catalyst. The series connection between unit c-Si IBC solar cells was brief, unlike that of existing conventional c-Si solar cells; therefore, the ohmic loss caused by the resistance of the connection electrode was reduced to a minimum. Additionally, we demonstrated a seamless all-in-one solar system, with a minimized efficiency loss (similar to a natural leaf); the loss was minimal because no additional space was required for module fabrication. This advantage promotes the compact manufacture encapsulation of the module and prevents corrosion of the c-Si in the electrolyte. Accordingly, the fabricated c-Si IBC photoanode was stable for 3 days and the STH efficiency was 10.1%. Notably, we developed a c-Si IBC module-based wireless all-in-one PEC device (artificial leaf), with an STH efficiency of 8.4%, which is higher than the efficiency of a natural leaf (0.1–1%), and even higher than that of C4 plants (4.3– 6%).

Data Availability Statement

The data that support the findings of this study are available from the corresponding authors upon reasonable request.

CRediT authorship contribution statement

Wonjoo Jin: Conceptualization, Data curation, Investigation, Formal analysis, Validation, Writing – original draft. **Changhwan Shin:** Conceptualization, Data curation, Investigation, Formal analysis, Validation, Writing – original draft, Writing. **Seyeon Lim:** Formal analysis, Validation. **Kangmin Lee:** Formal analysis, Validation. **Je Min Yu:** Formal analysis, Validation. **Kwanyong Seo:** Conceptualization, Validation, Writing – review & editing, Funding acquisition. **Ji-Wook Jang:** Conceptualization, Validation, Writing – review & editing, Funding acquisition.

Declaration of Competing Interest

The authors declare that they have no known competing financial interests or personal relationships that could have appeared to influence the work reported in this paper.

Data availability

Data will be made available on request.

Acknowledgments

W.J. and C.S. contributed equally to this work. This research was supported by the National Research Foundation (NRF), funded by Ministry of Science and ICT Planning [grant nos.: 2016K1A4A4A01922028, NRF-2019M1A2A2065614, NRF-2019R1A2C2086602, NRF-2020R1A4A1019568, 2021R1C1C1012258, 2022H1D3A3A01081140, and 2021M3H4A1A03051383], and by the Research Fund of the Ulsan National Institute of Science and Technology (UNIST) [grant no. 1.220022.01]. This work is supported by Alchemist project funded by Ministry of Trade, Industry and Energy thorough the Korean Evaluation Institute of Industrial Technology (1415180860 (20019321)).

Appendix A. Supporting information

Supplementary data associated with this article can be found in the online version at doi:10.1016/j.apcatb.2022.122086.

References

[1] N.S. Lewis, Research opportunities to advance solar energy utilization, Science 351 (2016) aad1920.
[2] D.G. Nocera, The artificial leaf, Acc. Chem. Res. 45 (2012) 767–776.
[3] S.A. Bonke, M. Wiechen, D.R. MacFarlane, L. Spiccia, Renewable fuels from concentrated solar power: towards practical artificial photosynthesis, Energy Environ. Sci. 8 (2015) 2791–2796.
[4] J.H. Kim, D. Hansora, P. Sharma, J.-W. Jang, J.S. Lee, Toward practical solar hydrogen production–an artificial photosynthetic leaf-to-farm challenge, Chem. Soc. Rev. 48 (2019) 1908–1971.
[5] M.G. Walter, E.L. Warren, J.R. McKone, S.W. Boettcher, Q. Mi, E.A. Santori, N. S. Lewis, Solar Water Splitting Cells, Chem. Rev. 110 (2010) 6446–6473.
[6] K. Sivula, R. van de Krol, Semiconducting materials for photoelectrochemical energy conversion, Nat. Rev. Mater. 1 (2016) 15010.
[7] J. Jin, K. Walczak, M.R. Singh, C. Karp, N.S. Lewis, C. Xiang, An experimental and modeling/simulation-based evaluation of the efficiency and operational performance characteristics of an integrated, membrane-free, neutral pH solar-driven water-splitting system, Energy Environ. Sci. 7 (2014) 3371–3380.
[8] P. Bogdanoff, D. Stellmach, O. Gabriel, B. Stannowski, R. Schlatmann, R. van de Krol, S. Fiechter, Artificial Leaf for Water Splitting Based on a Triple-Junction Thin-Film Silicon Solar Cell and a PEDOT:PSS/Catalyst Blend, Energy Technol. 4 (2016) 230–241.
[9] S.Y. Reece, J.A. Hamel, K. Sung, T.D. Jarvi, A.J. Esswein, J.J.H. Pijpers, D. G. Nocera, Wireless solar water splitting using silicon-based semiconductors and earth-abundant catalysts, Science 334 (2011) 645–648.
[10] K.S. Joya, Y.F. Joya, K. Ocakoglu, R. van de Krol, Water-splitting catalysis and solar fuel devices: artificial leaves on the move, Angew. Chem. Int. Ed. 52 (2013) 10426–10437.
[11] J. Rongé, T. Bosserez, D. Martel, C. Nervi, L. Boarino, F. Taulelle, G. Decher, S. Bordiga, J.A. Martens, Monolithic cells for solar fuels, Chem. Soc. Rev. 43 (2014) 7963–7981.
[12] B.A. Pinaud, J.D. Benck, L.C. Seitz, A.J. Forman, Z. Chen, T.G. Deutsch, B.D. James, K.N. Baum, G.N. Baum, S. Ardo, H. Wang, E. Miller, T.F. Jaramillo, Technical and economic feasibility of centralized facilities for solar hydrogen production via photocatalysis and photoelectrochemistry, Energy Environ. Sci. 6 (2013) 1983–2002.
[13] M.R. Shaner, H.A. Atwater, N.S. Lewis, E.W. McFarland, A comparative technoeconomic analysis of renewable hydrogen production using solar energy, Energy Environ. Sci. 9 (2016) 2354–2371.
[14] W.J.C. Vijselaar, P. Perez-Rodriguez, P.J. Westerik, R.M. Tiggelaar, A.H.M. Smets, H. Gardeniers, J. Huskens, A Stand-Alone Si-Based Porous Photoelectrochemical Cell, Adv. Energy Mater. 9 (2019), 1803548.
[15] T. Sekimoto, H. Hashiba, S. Shinagawa, Y. Uetake, M. Deguchi, S. Yotsuhashi, K. Ohkawa, Wireless InGaN–Si/Pt device for photo-electrochemical water splitting, Jpn. J. Appl. Phys. 55 (2016), 088004.
[16] K. Walczak, Y. Chen, C. Karp, J.W. Beeman, M. Shaner, J. Spurgeon, I.D. Sharp, X. Amashukeli, W. West, J. Jin, N.S. Lewis, C. Xiang, Modeling, Simulation, and Fabrication of a Fully Integrated, Acid-stable, Scalable Solar-Driven Water-Splitting System, ChemSusChem 8 (2015) 544–551.
[17] K. Sun, S. Shen, Y. Liang, P.E. Burrows, S.S. Mao, D. Wang, Enabling silicon for solar-fuel production, Chem. Rev. 114 (2014) 8662–8719.
[18] M.R. Shaner, J.R. McKone, H.B. Gray, N.S. Lewis, Functional integration of Ni–Mo electrocatalysts with Si microwire array photocathodes to simultaneously achieve high fill factors and light-limited photocurrent densities for solar-driven hydrogen evolution, Energy Environ. Sci. 8 (2015) 2977–2984.
[19] T. Weier, C. Stocking, The chloroplast: structure, inheritance, and enzymology. II, Bot. Rev. 18 (1952) 14–75.
[20] R.E. Blankenship, D.M. Tiede, J. Barber, G.W. Brudvig, G. Fleming, M. Ghirardi, M. R. Gunner, W. Junge, D.M. Kramer, A. Melis, T.A. Moore, C.C. Moser, D.G. Nocera, A.J. Nozik, D.R. Ort, W.W. Parson, R.C. Prince, R.T. Sayre, Comparing Photosynthetic and Photovoltaic Efficiencies and Recognizing the Potential for Improvement, Science 332 (2011) 805–809.
[21] R. Sager, G.E. Palade, Structure and development of the chloroplast in Chlamydomonas: I. The normal green cell, J. Cell Biol. 3 (1957) 463–488.
[22] H.-D. Um, N. Kim, K. Lee, I. Hwang, J.H. Seo, K. Seo, Dopant-Free All-Back-Contact Si Nanohole Solar Cells Using MoOx and LiF Films, Nano Lett. 16 (2016) 981–987.
[23] L. Trotochaud, J.K. Ranney, K.N. Williams, S.W. Boettcher, Solution-Cast Metal Oxide Thin Film Electrocatalysts for Oxygen Evolution, J. Am. Chem. Soc. 134 (2012) 17253–17261.
[24] M. Gao, W. Sheng, Z. Zhuang, Q. Fang, S. Gu, J. Jiang, Y. Yan, Efficient Water Oxidation Using Nanostructured α-Nickel-Hydroxide as an Electrocatalyst, J. Am. Chem. Soc. 136 (2014) 7077–7084.
[25] T.-Y. Jeon, S.K. Kim, N. Pinna, A. Sharma, J. Park, S.Y. Lee, H.C. Lee, S.-W. Kang, H.-K. Lee, H.H. Lee, Selective dissolution of surface nickel close to platinum in PtNi nanocatalyst toward oxygen reduction reaction, Chem. Mater. 28 (2016) 1879–1887.
[26] U. De Silva, J. Masud, N. Zhang, Y. Hong, W.P.R. Liyanage, M. Asle Zaeem, M. Nath, Nickel telluride as a bifunctional electrocatalyst for efficient water splitting in alkaline medium, J. Mater. Chem. A 6 (2018) 7608–7622.
[27] S.A. Lee, I.J. Park, J.W. Yang, J. Park, T.H. Lee, C. Kim, J. Moon, J.Y. Kim, H. W. Jang, Electrodeposited Heterogeneous Nickel-Based Catalysts on Silicon for Efficient Sunlight-Assisted Water Splitting, Cell Rep. Phys. Sci. 1 (2020), 100219.
[28] H. Sun, Y. Lian, C. Yang, L. Xiong, P. Qi, Q. Mu, X. Zhao, J. Guo, Z. Deng, Y. Peng, A hierarchical nickel–carbon structure templated by metal–organic frameworks for efficient overall water splitting, Energy Environ. Sci. 11 (2018) 2363–2371.
[29] N. Weidler, J. Schuch, F. Knaus, P. Stenner, S. Hoch, A. Maljusch, R. Schäfer, B. Kaiser, W. Jaegermann, X-ray Photoelectron Spectroscopic Investigation of Plasma-Enhanced Chemical Vapor Deposited NiOx, NiOx(OH)y, and CoNiOx(OH)y: Influence of the Chemical Composition on the Catalytic Activity for the Oxygen Evolution Reaction, J. Phys. Chem. C. 121 (2017) 6455–6463.

[30] L.S. Bezerra, G. Maia, Developing efficient catalysts for the OER and ORR using a combination of Co, Ni, and Pt oxides along with graphene nanoribbons and NiCo2O4, J. Mater. Chem. A 8 (2020) 17691–17705.
[31] K.L. Nardi, N. Yang, C.F. Dickens, A.L. Strickler, S.F. Bent, Creating Highly Active Atomic Layer Deposited NiO Electrocatalysts for the Oxygen Evolution Reaction, Adv. Energy Mater. 5 (2015), 1500412.
[32] D. Walker, Biofuels, facts, fantasy, and feasibility, J. Appl. Phycol. 21 (2009) 509–517.
[33] X.-G. Zhu, S.P. Long, D.R. Ort, Improving photosynthetic efficiency for greater yield, Annu. Rev. Plant Biol. 61 (2010) 235–261.